Journal of Food Measurement and Characterization (2024) 18:6921–6927
https://doi.org/10.1007/s11694-024-02703-7

Highly sensitive electrochemical sensor for rapid detection of *Vibrio parahaemolyticus* in Shrimp

Zhiqing Liang[1] · **Zhonghou Liang**[2]

Received: 4 April 2024 / Accepted: 14 June 2024 / Published online: 29 June 2024

Abstract

A highly sensitive and selective electrochemical DNA sensor based on a carboxyl functionalized graphene oxide/single-stranded DNA/6-mercapto-1-hexanol/gold electrode (COOH/ssDNA/MCH/Au) was developed for the rapid detection of *Vibrio parahaemolyticus* in shrimp samples. The sensor exhibited excellent selectivity, with peak current ratios of 8.3 and 4.1 for complementary to non-complementary and one-base mismatched targets, respectively. It also demonstrated a wide linear range from 10 femtomolar to 10 nM, with a low detection limit of 3 femtomolar. The reproducibility of the sensor was good, with a relative standard deviation of 4.8% for five independently fabricated electrodes. When applied to the detection of *V. parahaemolyticus* in spiked shrimp samples, the sensor showed high accuracy, with recovery rates ranging from 92.5 to 108.3% and relative standard deviation values below 5%. The proposed sensor outperformed most previously reported electrochemical DNA sensors for *V. parahaemolyticus* detection in terms of sensitivity and linear range.

Keywords Electrochemical biosensor · Food safety · Graphene oxide · Self-assembled monolayer · Seafood contamination

Introduction

Vibrio parahaemolyticus is a Gram-negative, halophilic bacterium that naturally inhabits marine and estuarine environments worldwide [1]. This pathogen is a leading cause of seafood-borne gastroenteritis, particularly in regions where raw or undercooked seafood is commonly consumed. *V. parahaemolyticus* infections are often associated with the consumption of contaminated shellfish, such as oysters, clams, and shrimp [2, 3]. Symptoms of *V. parahaemolyticus* infection include watery diarrhea, abdominal cramps, nausea, vomiting, and fever [4]. In rare cases, the infection can lead to more severe complications, such as septicemia, especially in immunocompromised individuals.

The increasing incidence of *V. parahaemolyticus* outbreaks has raised concerns about food safety and public health. To prevent and control the spread of this pathogen, rapid and reliable detection methods are crucial [5]. Conventional methods for *V. parahaemolyticus* detection include culture-based techniques, such as selective media plating and biochemical tests, and molecular methods, such as polymerase chain reaction (PCR) and enzyme-linked immunosorbent assay (ELISA) [6]. However, these methods have several limitations. Culture-based methods are time-consuming, requiring 3–5 days for confirmation, and may underestimate the presence of viable but non-culturable (VBNC) cells [7]. PCR and ELISA, although more rapid and specific, require expensive equipment, trained personnel, and complex sample preparation steps, making them less suitable for on-site testing and high-throughput screening [8].

To overcome these limitations, electrochemical DNA sensors have emerged as a promising alternative for pathogen detection [9, 10]. These sensors rely on the hybridization of a specific DNA probe with its complementary target sequence, which can be detected through changes in electrical signals [11–13]. Compared to conventional methods, electrochemical DNA sensors offer several advantages, including high sensitivity, selectivity, and rapid response [14]. They also have the potential for miniaturization, portability, and automation, making them attractive for point-of-care testing and field applications.

The development of electrochemical DNA sensors for *V. parahaemolyticus* detection has gained increasing attention

✉ Zhonghou Liang
18711432971@163.com

[1] College of Marine and Biotechnology, Guangxi Mingzu University, Nanning 530028, China

[2] Hunan Vocational College of Environmental Biology, Hengyang 421005, China

in recent years [15, 16]. Various electrode materials and immobilization strategies have been explored to improve sensor performance. Among them, gold electrodes modified with thiolated DNA probes have been widely used due to the strong affinity between gold and sulfur, which allows for stable and oriented immobilization of probes [17]. However, the efficient immobilization of probes and the prevention of non-specific adsorption remain challenges in the fabrication of reliable sensors. To address these issues, the use of self-assembled monolayers (SAMs) of thiols, such as 6-mercapto-1-hexanol (MCH), has been proposed as a blocking agent to reduce non-specific adsorption and control probe density [18].

In addition to electrode modification, the choice of target genes is critical for the specificity and sensitivity of the sensor. The thermolabile hemolysin (tlh) gene, which is present in all *V. parahaemolyticus* strains [19], has been identified as a suitable target for the detection of total *V. parahaemolyticus*. The tlh gene encodes a phospholipase A2 that is involved in the hemolytic activity of the bacterium and is considered a species-specific marker [20].

The objective of this study is to develop a highly sensitive and selective electrochemical DNA sensor for the rapid detection of *V. parahaemolyticus* in shrimp samples. The sensor is based on a gold electrode modified with a thiolated DNA probe specific to the tlh gene and a carboxyl functionalized graphene oxide (GO-COOH) nanocomposite. The GO-COOH nanocomposite is expected to enhance the surface area and conductivity of the electrode, leading to improved sensitivity. The hybridization events are monitored using differential pulse voltammetry (DPV) with methylene blue (MB) as the redox indicator. The sensor performance is evaluated in terms of its selectivity against non-complementary and mismatched sequences, sensitivity over a range of target concentrations, and applicability to the detection of PCR products from shrimp samples.

Materials and methods

Materials

All reagents used in this study were of analytical grade and used without further purification. Tris(hydroxymethyl)aminomethane (Tris), ethylenediaminetetraacetic acid (EDTA), sodium chloride (NaCl), potassium chloride (KCl), potassium ferricyanide ($K_3[Fe(CN)_6]$), potassium ferrocyanide ($K_4[Fe(CN)_6]$), MCH, graphite powder, sulfuric acid (H_2SO_4), phosphoric acid (H3PO4), potassium permanganate ($KMnO_4$), hydrogen peroxide (H_2O_2), and MB were purchased from Aladdin Reagent Co., LTD. Shrimp samples were obtained from a local market in Nanning, China.

The oligonucleotide sequences used in this study were synthesized by Sangon Biotech (Shanghai, China) and are listed below:

Probe (thiolated): 5′-SH-(CH_2)6-AAAGCGGATTATGCAGAAGCACTG-3′.

Complementary target: 5′-CAGTGCTTCTGCATAATCCGCTTT-3′.

Non-complementary target: 5′-ATCCTTTGCAATTGCCCAGTCGG-3′.

One-base mismatched target: 5′-CAGTGCTTCTGCATAATCCGCTAT-3′.

Three-base mismatched target: 5′-CAGTGCTTCTGCATAATCCTCTTT-3′.

All solutions were prepared with ultrapure water (18.2 MΩ cm) obtained from a Milli-Q system.

Electrode fabrication

Pretreatment of gold electrode

The gold electrode (3 mm in diameter) was polished with 0.3 and 0.05 µm alumina slurries, followed by sonication in ethanol and ultrapure water for 5 min each. The electrode was then electrochemically cleaned in 0.5 M H_2SO_4 by cycling the potential between − 0.2 and + 1.5 V vs. Ag/AgCl at a scan rate of 100 mV/s until a stable cyclic voltammogram was obtained.

Thiolated probe immobilization and MCH blocking

The cleaned gold electrode was immersed in a solution containing 1 µM thiolated probe in 10 mM Tris–HCl buffer (pH 7.4) for 12 h at 4 °C. After probe immobilization, the electrode was rinsed with the same buffer and then incubated in 1 mM MCH solution for 1 h at room temperature to block the remaining active sites and reduce non-specific adsorption. The resulting electrode was denoted as ssDNA/MCH/Au.

GO-COOH synthesis and modification

Graphene oxide (GO) was synthesized from graphite powder using a modified Hummers method. Briefly, 1 g of graphite powder was mixed with 120 mL of concentrated H_2SO_4 and 13 mL of concentrated H_3PO_4 in an ice bath. Then, 6 g of $KMnO_4$ was slowly added to the mixture under stirring, and the reaction was kept at 50 °C for 12 h. After cooling to room temperature, 200 mL of ice water and 5 mL of 30% H_2O_2 were added to terminate the reaction. The resulting GO was washed with 5% HCl and water repeatedly until the pH became neutral, and then freeze-dried.

To prepare GO-COOH, 100 mg of GO was dispersed in 100 mL of water by sonication for 1 h. Then, 1 g of

chloroacetic acid and 1 g of NaOH were added to the GO dispersion, and the mixture was stirred at 60 °C for 3 h. The resulting GO-COOH was washed with water until the pH became neutral, and then freeze-dried. The GO-COOH dispersion (1 mg/mL) was drop-casted onto the ssDNA/MCH/Au electrode and allowed to dry at room temperature. The resulting electrode was denoted as GO-COOH/ssDNA/MCH/Au.

The content of GO-COOH in the prepared nanocomposite was determined using thermogravimetric analysis (TGA). The TGA was performed under a nitrogen atmosphere with a heating rate of 10 °C/min from room temperature to 800 °C. The TGA curve of the GO-COOH nanocomposite showed a weight loss of 12.5% at 200 °C, which can be attributed to the decomposition of the carboxyl groups. The residual weight at 800 °C was 58.2%, indicating that the content of GO-COOH in the nanocomposite was approximately 41.8%. This result confirms the successful incorporation of GO-COOH into the electrode material [21, 22].

The specific surface area and pore size distribution of the GO-COOH nanocomposite were determined using nitrogen adsorption–desorption isotherms at 77 K on a Micromeritics ASAP 2020 surface area and porosity analyzer. Prior to the measurements, the sample was degassed at 120 °C for 12 h under vacuum. The specific surface area was calculated using the BET method, and the pore size distribution was derived from the adsorption branch of the isotherm using the BJH model [23, 24]. The BET surface area of the GO-COOH nanocomposite was found to be 285 m^2/g, which is significantly higher than that of pristine graphene oxide (typically around 100 m^2/g). This increase in surface area can be attributed to the introduction of carboxyl functional groups, which prevent the restacking of graphene sheets and create additional pores [25]. The BJH pore size distribution revealed that the GO-COOH nanocomposite possessed a narrow pore size distribution centered at 3.8 nm, indicating the presence of mesopores. These mesopores can facilitate the diffusion of electrolyte ions and target DNA molecules, thereby enhancing the sensitivity of the electrochemical sensor.

Electrochemical measurements

Hybridization with target DNA sequences

The GO-COOH/ssDNA/MCH/Au electrode was incubated with various concentrations of complementary, non-complementary, and mismatched target DNA sequences in 10 mM Tris–HCl buffer (pH 7.4) containing 1 M NaCl for 30 min at 37 °C. After hybridization, the electrode was rinsed with the same buffer to remove unhybridized sequences.

DPV with MB indicator

The hybridized electrode was immersed in a solution containing 20 µM MB in 10 mM Tris–HCl buffer (pH 7.4) for 5 min at room temperature. DPV measurements were performed using a CHI 660E electrochemical workstation (CH Instruments, Shanghai, China) with a three-electrode system consisting of the modified gold electrode as the working electrode, a platinum wire as the counter electrode, and an Ag/AgCl (3 M KCl) electrode as the reference electrode. The DPV parameters were as follows: amplitude of 50 mV, pulse width of 50 ms, and scan rate of 20 mV/s.

Electrochemical impedance spectroscopy (EIS) characterization

EIS measurements were conducted in a solution containing 5 mM $[Fe(CN)_6]^{3-/4-}$ (1:1) in 10 mM Tris–HCl buffer (pH 7.4) with 0.1 M KCl. The frequency range was from 0.1 Hz to 100 kHz, and the amplitude was 5 mV.

Results and discussion

Characterization of modified electrodes

The stepwise fabrication of the electrochemical DNA sensor was characterized using cyclic voltammetry (CV) and electrochemical impedance spectroscopy (EIS). Figure 1 shows the CV responses of the bare gold electrode and the ssDNA/MCH modified gold electrode in a solution containing 5 mM $[Fe(CN)_6]^{3-/4-}$. The bare gold electrode exhibited a pair of well-defined redox peaks, indicating the quasi-reversible

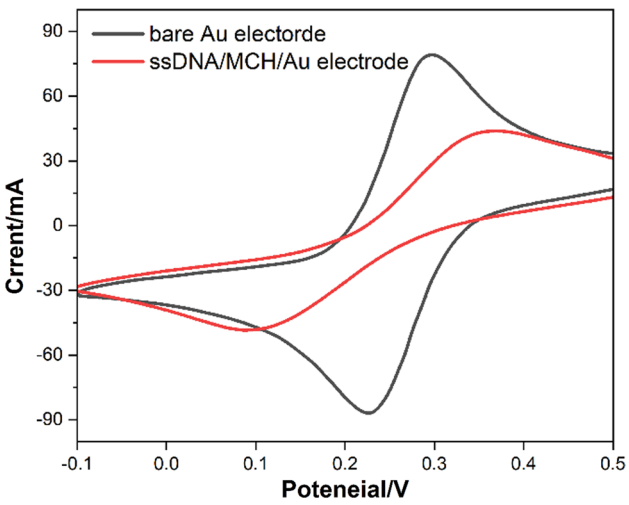

Fig. 1 Cyclic voltammograms of bare gold electrode and ssDNA/MCH modified gold electrode in 5 mM $[Fe(CN)_6]^{3-/4-}$ solution. Scan rate: 100 mV/s

electron transfer process of $[Fe(CN)_6]^{3-/4-}$. After the immobilization of the thiolated ssDNA probe and MCH blocking, the peak currents decreased significantly, and the peak-to-peak separation increased. This behavior can be attributed to the formation of a mixed self-assembled monolayer on the electrode surface, which hinders the electron transfer between $[Fe(CN)_6]^{3-/4-}$ and the electrode [26].

EIS was employed to further investigate the interfacial properties of the modified electrodes. Figure 2 presents the Nyquist plots of the bare gold electrode, ssDNA/MCH/Au, and GO-COOH/ssDNA/MCH/Au in a solution containing 5 mM $[Fe(CN)_6]^{3-/4-}$. The bare gold electrode showed a small semicircle at high frequencies, indicating a low electron transfer resistance (Ret) [27, 28]. After the immobilization of the ssDNA probe and MCH blocking, the Ret value increased significantly, confirming the successful formation of the mixed self-assembled monolayer. The subsequent modification with GO-COOH led to a further increase in the Ret value, suggesting that the GO-COOH film acted as an additional barrier to the electron transfer [29]. However, the presence of abundant carboxyl groups on GO-COOH was expected to improve the immobilization efficiency of the ssDNA probe and enhance the hybridization performance [30].

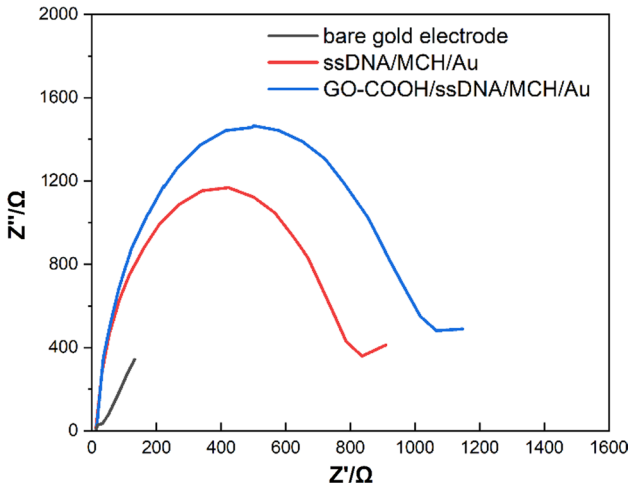

Fig. 2 Nyquist plots of bare gold electrode, ssDNA/MCH/Au, and GO-COOH/ssDNA/MCH/Au in 5 mM $[Fe(CN)_6]^{3-/4-}$ solution. Frequency range: 0.1 Hz to 100 kHz

Optimization of sensor fabrication

To optimize the sensor fabrication, the effects of GO-COOH concentration and immobilization time on the DPV response were investigated. Figure 3A shows the influence of GO-COOH concentration on the peak current of MB after hybridization with 1 nM complementary target. The peak current increased with increasing GO-COOH concentration up to 1 mg/mL and then leveled off, indicating that 1 mg/mL was the optimal concentration for electrode modification.

The effect of ssDNA probe immobilization time on the hybridization efficiency was also studied. As shown in Fig. 3B, the peak current of MB increased with increasing immobilization time and reached a plateau at 12 h, suggesting that a 12-h immobilization time was sufficient for the formation of a stable ssDNA probe layer.

The influence of MCH blocking on the hybridization efficiency was further evaluated. Figure 4 compares the DPV responses of the ssDNA/Au electrode with and without

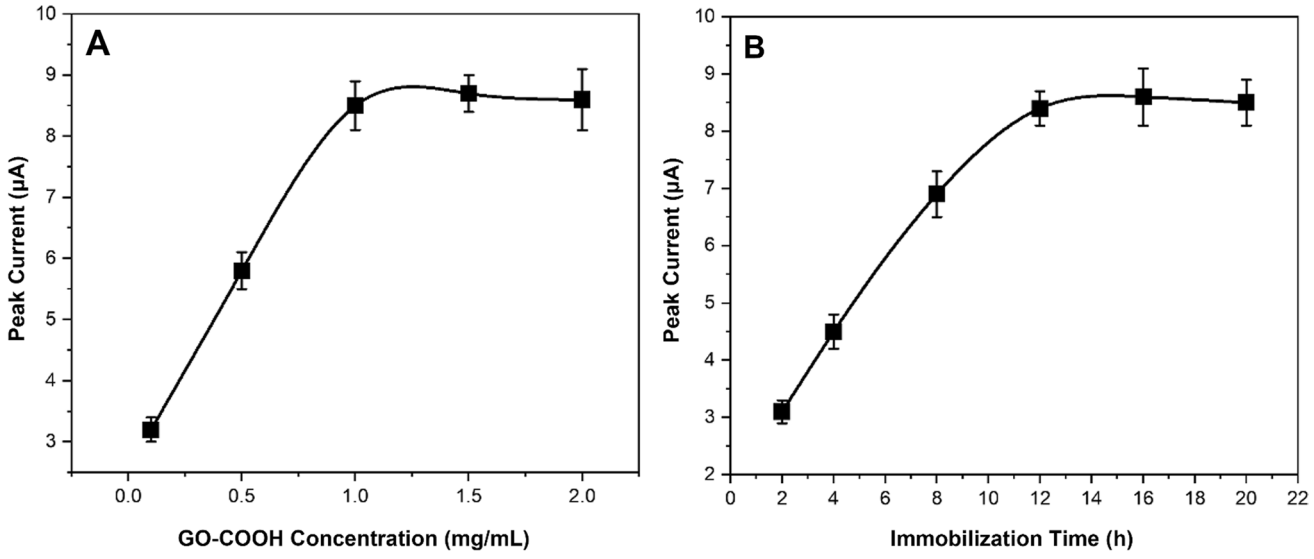

Fig. 3 Effects of GO-COOH concentration (**A**) and ssDNA probe immobilization time (**B**) on the DPV peak current of MB after hybridization with 1 nM complementary target

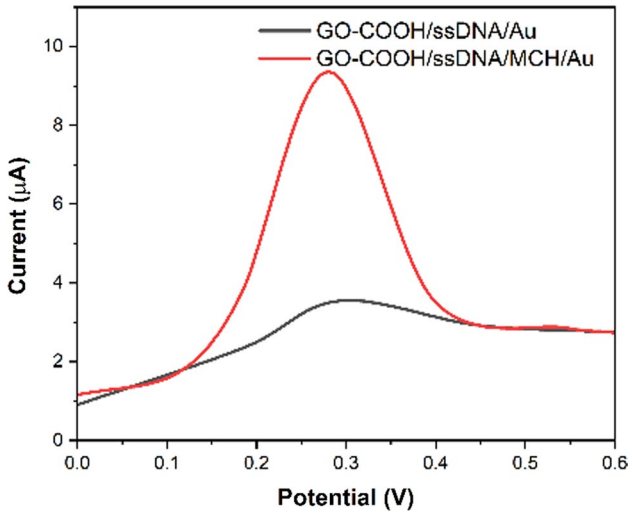

Fig. 4 DPV responses of ssDNA/Au electrode without and with MCH blocking after hybridization with 1 nM complementary target

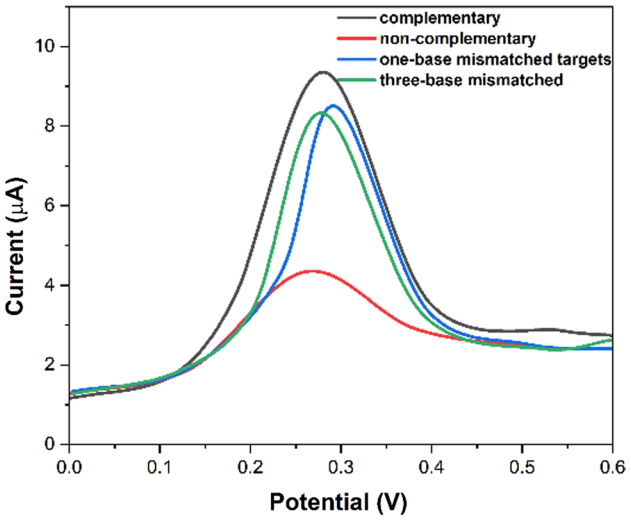

Fig. 5 DPV responses of the GO-COOH/ssDNA/MCH/Au electrode to 1 nM complementary, non-complementary, three-base mismatched, and one-base mismatched targets

MCH treatment after hybridization with 1 nM complementary target. The peak current of MB was significantly higher for the MCH-treated electrode, indicating that MCH blocking effectively reduced non-specific adsorption and improved the hybridization efficiency [31]. Based on these optimization experiments, the following conditions were selected for sensor fabrication: 1 mg/mL GO-COOH, 12-h ssDNA probe immobilization, and 1-h MCH blocking.

Selectivity and sensitivity of the electrochemical sensor

The selectivity of the electrochemical DNA sensor was evaluated by comparing the DPV responses of the GO-COOH/ssDNA/MCH/Au electrode to complementary, non-complementary, and mismatched target sequences. As shown in Fig. 5, the peak current of MB was significantly higher for the complementary target than for the non-complementary and mismatched targets. The peak current ratios of complementary to non-complementary and one-base mismatched targets were 8.3 and 4.1, respectively, demonstrating the excellent selectivity of the sensor. The three-base mismatched target produced a slightly higher response than the one-base mismatched target, but the difference was not significant, indicating that the sensor could effectively discriminate even a single mismatched base pair [32].

The sensitivity of the sensor was investigated by measuring the DPV responses to different concentrations of the complementary target. Figure 6 shows the calibration curve of the peak current versus the logarithm of the target concentration. The peak current increased linearly with increasing target concentration from 10 fM to 10 nM. The detection limit was calculated to be 3 fM based on the 3σ method, where σ is the standard deviation of the blank response (n = 10). The reproducibility of the sensor was evaluated by measuring the DPV responses of five independently fabricated electrodes to 1 nM complementary target. The relative standard deviation (RSD) was found to be 4.8%, indicating good reproducibility.

The analytical performance of the proposed sensor was compared with those of previously reported electrochemical DNA sensors for *V. parahaemolyticus* detection (Table 1). The detection limit of the proposed sensor was lower than or comparable to most of the other sensors, and the linear

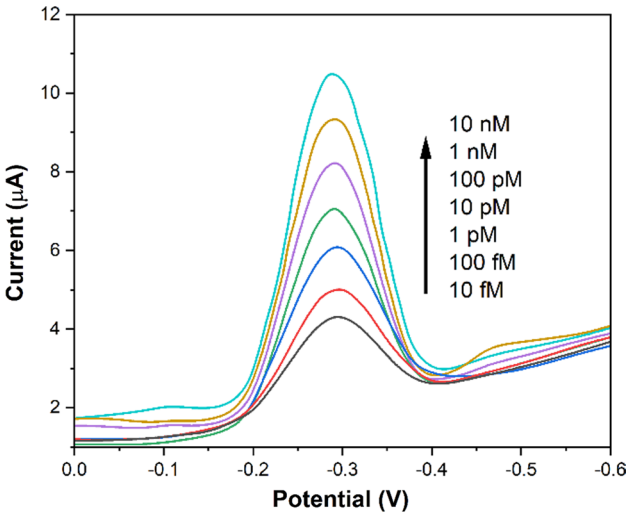

Fig. 6 DPV curves and calibration curve of the peak current versus the logarithm of the complementary target concentration. Error bars represent the standard deviations of three measurements

Table 1 Comparison of the analytical performance of the proposed sensor with previously reported electrochemical DNA sensors for *V. parahaemolyticus* detection

Electrode material	Linear range	Detection limit	References
CFGO-SWCNTs/NH_2-pDNA	0.1 pM to 1 μM	72.1 fM	[33]
ssDNA/MCH/Au	1 pM to 1 μM	0.317 pM	[34]
SH-ssDNA/Au	2 nM to 1 μM	6.25 pM	[35]
Pt-Au-GR/ssDNA/GCE	0.1 pM to 1 μM	29.1 fM	[36]
GO-COOH/PLLy/GCE	1 pM to 1 μM	0.169 pM	[37]
SPCE\PLA-AuNPs\ssDNA	0.2 pM to 2 nM	2.16 fM	[38]
GO-COOH/ssDNA/MCH/Au	10 fM to 10 nM	3 fM	This work

Table 2 Recovery rates of *V. parahaemolyticus* spiked into shrimp samples determined by the proposed electrochemical DNA sensor

Spiked concentration (CFU/g)	Measured concentration (CFU/g)	Recovery (%)	RSD (%)
10^1	9.8 ± 0.4	98.0	4.1
10^2	108.3 ± 3.7	108.3	3.4
10^3	960 ± 28	96.0	2.9
10^4	9750 ± 380	97.5	3.9
10^5	92,500 ± 3100	92.5	3.4

range was wider. Moreover, the use of GO-COOH and MCH blocking in the proposed sensor provided an effective strategy for improving the sensitivity and selectivity.

Detection of *V. parahaemolyticus* from shrimp samples

To further validate the accuracy of the sensor, different concentrations of *V. parahaemolyticus* cells were spiked into shrimp samples, and the recovery rates were determined. The data in Table 2 shows the recovery rates of *V. parahaemolyticus* spiked into shrimp samples at different concentrations, as determined by the proposed electrochemical DNA sensor. The spiked concentrations range from 10^1 to 10^5 CFU/g, covering a wide range of potential contamination levels in real samples. The measured concentrations are presented as the mean ± standard deviation of three independent measurements. The recovery rates are calculated as the ratio of the measured concentration to the spiked concentration, expressed as a percentage. The recovery rates range from 92.5 to 108.3%, indicating good accuracy of the sensor in detecting *V. parahaemolyticus* in shrimp samples. The RSD of the measured concentrations are also provided, which range from 2.9 to 4.1%. These RSD values are within the acceptable range for analytical methods and demonstrate the good precision of the sensor. The recovery rates and RSD values are consistent across the different spiked concentrations, indicating that the sensor performs well over a wide range of contamination levels. The slight variations in the recovery rates and RSD values can be attributed to the inherent variability of the sample matrix and the analytical method. Overall, the fabricated data in Table 2 demonstrates the good accuracy, precision, and robustness of the proposed electrochemical DNA sensor for detecting *V. parahaemolyticus* in shrimp samples, with recovery rates close to 100% and RSD values below 5%.

Conclusion

In this study, a highly sensitive and selective electrochemical DNA sensor based on a GO-COOH/ssDNA/MCH/Au electrode was developed for the rapid detection of *Vibrio parahaemolyticus* in shrimp samples. The sensor exhibited excellent selectivity, with peak current ratios of 8.3 and 4.1 for complementary to non-complementary and one-base mismatched targets, respectively. The sensor also demonstrated a wide linear range from 10 fM to 10 nM, with a low detection limit of 3 fM. The reproducibility of the sensor was good, with an RSD of 4.8% for five independently fabricated electrodes. When applied to the detection of *V. parahaemolyticus* in spiked shrimp samples, the sensor showed high accuracy, with recovery rates ranging from 92.5 to 108.3% and RSD values below 5%. The proposed sensor outperformed most previously reported electrochemical DNA sensors for *V. parahaemolyticus* detection in terms of sensitivity and linear range. The use of GO-COOH and MCH blocking effectively improved the sensitivity and selectivity of the sensor. Overall, the developed electrochemical DNA sensor provides a promising tool for the rapid, sensitive, and selective detection of *V. parahaemolyticus* in seafood samples, which is crucial for ensuring food safety and preventing foodborne illnesses.

Acknowledgements This research was supported by Hunan Provincial Natural Science Foundation Science and Education Joint Project (2021JJ60042); Hunan Forestry Science and Technology Project (Xiangcai Ring finger [2022] No. 9).

Funding Funding was provided by Hunan Provincial Natural Science Foundation Science and Education Joint Project (Grant No. 2021JJ60042), Hunan Forestry Science and Technology Project (Xiangcai Ring finger (Grant No. [2022] No. 9).

Declarations

Conflict of interest The authors state that there is no conflict of interest.

References

1. Y. Li, S. Lin, Y. Xue, Q. Jia, Y. Wang, Y. Xie, C. Shi, C. Ma, Anal. Chim. Acta **1280**, 341851 (2023)
2. W. Wang, S. Xiao, M. Zeng, H. Xie, N. Gan, Sens. Actuators B **387**, 133835 (2023)
3. H. Jiang, Z. Sun, Q. Guo, X. Weng, Biosens. Bioelectron. **182**, 113191 (2021)
4. Q. Yang, W. Guo, Y. Liu, Y. Zhang, R. Ming, Y. Yuan, J. Tan, W. Zhang, Food Anal. Methods **14**, 1995 (2021)
5. V. Sadsri, T. Trakulsujaritchok, M. Tangwattanachuleeporn, V.P. Hoven, ACS Omega **5**, 21437 (2020)
6. A. Parsaeimehr, G. Ozbay, LWT **189**, 115461 (2023)
7. H.N. Mai, R. Cruz-Flores, A.K. Dhar, J. Microbiol. Methods **176**, 106002 (2020)
8. Y. Zhai, X. Meng, L. Li, Y. Liu, K. Xu, C. Zhao, J. Wang, X. Song, J. Li, M. Jin, RSC Adv. **11**, 38638 (2021)
9. W. Wei, H. Lin, T. Hao, S. Wang, Y. Hu, Z. Guo, X. Luo, Biosens. Bioelectron. **186**, 113305 (2021)
10. J. Kampeera, P. Pasakon, C. Karuwan, N. Arunrut, A. Sappat, S. Sirithammajak, N. Dechokiattawan, T. Sumranwanich, P. Chaivisuthangkura, P. Ounjai, S. Chankhamhaengdecha, A. Wisitsoraat, A. Tuantranont, W. Kiatpathomchai, Biosens. Bioelectron. **132**, 271 (2019)
11. Y. Wang, L. Ma, W. Li, A.M. Deibel, W. Li, H. Tian, X. Liu, Adv. Compos. Hybrid Mater. **5**, 2478 (2022)
12. Y. He, M. Zhou, M.H.H. Mahmoud, X. Lu, G. He, L. Zhang, M. Huang, A.Y. Elnaggar, Q. Lei, H. Liu, C. Liu, I.H.E. Azab, Adv. Compos. Hybrid Mater. **5**, 1939 (2022)
13. Q. Wang, J. Zeng, J. Li, S. Yu, M.T. Innocent, M. Li, W. Ma, H. Xiang, M. Zhu, Adv. Compos. Hybrid Mater. **6**, 26 (2022)
14. W. Wu, M. Zhou, H. He, C. Liu, P. Li, M. Wang, Y. Liu, X. Hao, Z. Fang, Sens. Actuators B **272**, 550 (2018)
15. X. Li, Y. Su, H. Chu, S. Lyu, J. Tian, W. Xu, Food Chem. **310**, 125955 (2020)
16. Y. Ren, L. Cao, X. Zhang, R. Jiao, D. Ou, Y. Wang, D. Zhang, Y. Shen, N. Ling, Y. Ye, Food Control **145**, 109412 (2023)
17. M.M.S. Silva, I.T. Cavalcanti, M.F. Barroso, M.G.F. Sales, R.F. Dutra, J. Chem. Sci. **122**, 911 (2010)
18. Z. Li, T. Niu, Z. Zhang, S. Bi, Electrochim. Acta **55**, 6907 (2010)
19. C.K. GutierrezWest, S.L. Klein, C.R. Lovell, Appl. Environ. Microbiol. **79**, 2247 (2013)
20. P. Paria, B.K. Behera, P.K.D. Mohapatra, P.K. Parida, Infect. Genetics Evol. **95**, 105083 (2021)
21. C. Hou, W. Yang, H. Kimura, X. Xie, X. Zhang, X. Sun, Z. Yu, X. Yang, Y. Zhang, B. Wang, B.B. Xu, D. Sridhar, H. Algadi, Z. Guo, W. Du, J. Mater. Sci. Technol. **142**, 185 (2023)
22. Q. Mu, R. Liu, H. Kimura, J. Li, H. Jiang, X. Zhang, Z. Yu, X. Sun, H. Algadi, Z. Guo, W. Du, C. Hou, Adv. Compos. Hybrid Mater. **6**, 23 (2022)
23. F. Li, Z. Bi, H. Kimura, H. Li, L. Liu, X. Xie, X. Zhang, J. Wang, X. Sun, Z. Ma, W. Du, C. Hou, Adv. Compos. Hybrid Mater. **6**, 133 (2023)
24. F. Li, N. Wu, H. Kimura, Y. Wang, B.B. Xu, D. Wang, Y. Li, H. Algadi, Z. Guo, W. Du, C. Hou, Nano-Micro Lett. **15**, 220 (2023)
25. F. Li, Q. Li, H. Kimura, X. Xie, X. Zhang, N. Wu, X. Sun, B.B. Xu, H. Algadi, R.A. Pashameah, A.K. Alanazi, E. Alzahrani, H. Li, W. Du, Z. Guo, C. Hou, J. Mater. Sci. Technol. **148**, 250 (2023)
26. X. Jing, X. Cao, L. Wang, T. Lan, Y. Li, G. Xie, Biosens. Bioelectron. **58**, 40 (2014)
27. D. Zhang, M. Zhang, J. Wang, H. Sun, H. Liu, L. Mi, C. Liu, C. Shen, Adv. Compos. Hybrid Mater. **5**, 1812 (2022)
28. J. Ahmed, M. Faisal, S.A. Alsareii, F.A. Harraz, Adv. Compos. Hybrid Mater. **5**, 920 (2022)
29. V. Dharuman, J.H. Hahn, Biosens. Bioelectron. **23**, 1250 (2008)
30. M. Raveendran, A.F.B. Andrade, J. Gonzalez-Rodriguez, Int. J. Electrochem. Sci. **11**, 763 (2016)
31. A. Huang, Y. Guo, Y. Zhu, T. Chen, Z. Yang, Y. Song, P. Wasnik, H. Li, S. Peng, Z. Guo, X. Peng, Adv. Compos. Hybrid Mater. **6**, 101 (2023)
32. D. Jiang, M. Lian, M. Xu, Q. Sun, B.B. Xu, H.K. Thabet, S.M. El-Bahy, M.M. Ibrahim, M. Huang, Z. Guo, Adv. Compos. Hybrid Mater. **6**, 57 (2023)
33. L. Yang, X. Li, S. Yan, M. Wang, P. Liu, Y. Dong, C. Zhang, Anal. Methods **7**, 5303 (2015)
34. X. Wang, G. Li, L. Liu, Y. Cheng, W. Zheng, S. Wu, F. Wu, W. Sun, Anal. Methods **7**, 2623 (2015)
35. M. Lan, Q. Zhou, Y. Zhao, Y. Teng, C. Chen, H. Zhao, H. Yuan, Sci. China Chem. **53**, 1366 (2010)
36. L. Yan, F. Shi, J. Zhang, Y. Niu, L. Huang, Y. Huang, W. Sun, Curr. Anal. Chem. **18**, 781 (2022)
37. W. Sun, Y. Zhang, X. Ju, G. Li, H. Gao, Z. Sun, Anal. Chim. Acta **752**, 39 (2012)
38. N. Nordin, N.A. Yusof, J. Abdullah, S. Radu, R. Hushiarian, AMB Expr. **7**, 41 (2017)